

*In memory of Academician Victor Panin,  
the founder of physical mesomechanics*

# The Physical Mesomechanics of the Earthquake Source

G. G. Kocharyan<sup>1\*</sup> and S. B. Kishkina<sup>1</sup>

<sup>1</sup>*Institute of Geosphere Dynamics, Russian Academy of Sciences, Moscow, 119334 Russia*

\* e-mail: [gevorgkidg@mail.ru](mailto:gevorgkidg@mail.ru)

Received November 02, 2020; revised November 02, 2020; accepted November 16, 2020

**Abstract**—This paper is a brief review of the main recent results obtained by studying fault slip processes. The published hypotheses and data are analyzed within the approach proposed by Panin, according to which the subsurface is considered as a multilevel hierarchically organized system where all processes evolve consistently at the nano-, micro-, meso- and macroscale levels. The review focuses on the hierarchy of structures that, according to modern concepts, form the seismogenic fault slip zone. The relationship of the structures with the mechanical characteristics of localized slip surfaces and microcontacts determining the slip dynamics of fault zones at the macrolevel is discussed. It is shown that the evolution of the contact properties of filler particles in the slip zone determines not only the occurrence of instability, but also the ability of a fault to recover strength with time. The simplest scheme of the hierarchy of macroscopic asperities is described to support the important principle that the initiation, evolution and arrest of a seismogenic fault depend on the size and relative position of regions with different dynamics of frictional characteristics during slip. The performed analysis of the results of field observations shows that because of the insufficient accuracy of observations and the ambiguous interpretation of the inverse problem solution, it is impossible to correctly identify fault segments with the velocity weakening property. The size and location of these zones can be more accurately determined from the analysis of records of high-frequency oscillations in the vicinity of an earthquake rupture. The basic principles of physical mesomechanics provide a good basis for the interpretation of such results.

*Keywords:* earthquake source, seismogenic faults, slip regimes, hierarchically organized medium, friction of geomaterials

**DOI:** 10.1134/S1029959921040019

## 1. INTRODUCTION

Geologists have long been aware that the Earth's crust, both on surface and in subsurface zones, contains a huge number of inhomogeneities and defects of various scales, from micro- and nanostructures to transcontinental faults. Geomorphologists [1, 2] drew attention to the regular hierarchy of crustal blocks, and later geophysicists introduced the corresponding hierarchy of deformation processes, physical and mechanical properties, and stress field parameters [3–5]. In so doing, the results derived within continuum mechanics were often inconsistent with the important local effects appearing mainly at structural boundaries.

In the 1980s and 1990s, V.E. Panin established a new scientific direction, physical mesomechanics [6–

8], which concerns with the self-consistent behavior of defects of all scales in a solid under deformation and seems to be applicable to the description of the deformation features studied in Earth sciences. Mesomechanics considers the medium, including the geomedium, as a multilevel hierarchically organized system, where all processes evolve self-consistently at the nano-, micro-, meso- and macroscale levels. In this case, the interfaces between regions with special properties are taken as functionally important subsystems [9].

An earthquake is caused by slip on a pre-existing geological fault. This is the main concept in the theory of earthquakes based on faulting, which was independently developed by Gilbert (1884) and Koto (1893) and generalized by Reid (1910). Within this

paradigm, cumulative displacement on the fault results from repeated sudden slips that occur at regular intervals on each active fault or its segment. Gilbert noted in his early works that an earthquake occurs when the stress accumulated on the fault becomes large enough to overcome the initial friction [10]. Later, probably when affected by investigations into cracking, friction faded into insignificance, and fracture at the earthquake source was associated with the crustal strength [11]. In such a model, earthquakes are caused by fracture in strong fault segments. Few or no earthquakes occur in weak, relatively low-strength, fault segments. This point of view is difficult to confirm experimentally because stresses in a particular site of the crust cannot be measured by seismological methods.

The situation changed radically when the alternative stick-slip mechanism was proposed in the fundamental work by Brace and Beyrlee [12]. By extending the sliding friction model, well known in mechanics, to the physics of faulting, an earthquake is thought of as a dynamically unstable slip occurring periodically on the fracture surface. In the stick-slip model, the seismicity of faults does not deal with strength, but depends on the stability or instability of the frictional properties of the fault, i.e. on the rate of friction variation with displacement or slip velocity as compared to the unloading rate of the host medium. In this case, the stress relieved during slip is reliably determined from the data of instrumental observations.

The resolution of modern seismological methods makes it possible not only to measure the average fault displacement and stress drop, but also to estimate their distribution both in time and in space. A variation of these parameters within a fault turns out to be very significant, which is undoubtedly associated with heterogeneity of the structure, frictional properties and stress on the fault plane.

In the second half of the 20th century, attempts to describe parameters of high-frequency motion observed in the near zone of an earthquake led to the development of an approach based on asperities. The latter are strong, stressed spots on the slip surface, which are surrounded by areas where stress is partially relieved during the interseismic period [13]. In the vicinity of these spots, the coseismic displacement is maximum, and the contribution of the seismic component to tectonic strains is close to unity.

Methods of seismology and tectonophysics, which deal with large spatial scales, are not yet able to adequately describe mechanical regularities of the proc-

ess of fault preparation, initiation, and arrest. They are limited for the most part to the statement and description of observation results [14], although there is some progress in this direction [15].

Slip during strong earthquakes occurs along faults hundreds of kilometers long, but dynamic weakening of friction that makes this slip possible is controlled by processes in a wide size range, from nano- to macroscales. In these regard, the fundamental principles of physical mesomechanics developed by Panin with the multilevel hierarchical approach to the analysis of deformation and fracture of solids can be extremely efficient in solving the problems of earthquake source physics.

This paper provides a brief review of the formulated concepts and recent results of investigations into fault slip processes.

## 2. GEOMETRY OF SLIP SURFACES IN ROCKS

When analyzing slip on continental faults, many specialists frequently address, explicitly or implicitly, a misleading description of asperities. These are taken as locking coarse irregularities in the contact zone, giving higher effective friction angles and adhesion in asperity zones.

Almost all tribological models of friction are primarily based on experiments with relatively smooth surfaces of structural materials. Nevertheless, stick-slip models and the dependence of the friction coefficient on the velocity and displacement, wear of surfaces, etc. are applicable to friction processes in rocks, at least in laboratory samples [16–18]. In so doing, the deduced results cannot be easily expand to slip regularities in cracks and faults up to several hundred kilometers in length on account of the pronounced scale dependence of rock and interface properties. Consideration should be given to the surface geometry and material properties at different hierarchical levels.

Any real surface has a definite topography, so that, when in contact, even almost flat surfaces touch each other only in some areas. The total area of true contact is rather small: the relation  $A_r \ll A$  holds up to high pressures, where  $A$  is the sample area, and  $A_r$  is the contact area.

Fault zones are no exception. The topography of exhumed fault surfaces and the geometry of crack and fault lines (their roughness) have been intensively studied [19, 20]. The intuitively clear concept of roughness is defined as a set of surface irregularities at a relatively small spacing within the limits of

the sampling length, providing a way to assess the surface roughness by contact measurement with a profilometer. The average roughness height is divided by the profile length: rougher surfaces have higher ratios. Similar methods for surface roughness measurement and evaluation, often used in classical mechanics, came into geophysical use in the middle of the 20th century. New roughness measurement methods have evolved by the end of the 20th century: noncontact methods, allowing for a significant increase in the measurement resolution down to fractions of nanometers. To do this, the surface is scanned by an ultra-thin probe/needle with the nanometer tip and by a laser beam reflected from the surface (atomic force microscopy, AFM). The probe moving across the surface can change the distance to the sample to keep the interaction value constant.

Numerous topographic measurements yield the relation of the surface roughness of real rocks to the scale of observations:

$$A_{av} = KL^\xi, \quad (1)$$

where  $A_{av}$  is the average asperity height on a scale  $L$ , and  $K$  is the constant factor [21–24]. Surfaces well described by the power law with  $\xi = 1$  are classed as self-similar surfaces, and surfaces with  $\xi \neq 1$  refer to self-affine surfaces [19, 25]. The exponent  $\xi$  in relation (1) is often called the roughness index.

Surface roughness was quantified on scales from fractions of nanometers to tens of meters in both natural objects and laboratory samples, for example, in [21–26]. It turned out that the roughness index is close to 0.80 for many fault surfaces. Thus, in [21, 27] it was shown that cracks from 1 to 1500 m in length, the roughness measurement results are best described by the dependence

$$A_{av} = 7.5 \times 10^{-3} L^{0.8}, \quad (2)$$

where the average amplitude of the profile deviation  $A_{av}$  and the block length  $L$  are measured in meters. Similar roughness values along parallel profiles of the fault, which are described by a self-affine geometry with the roughness index close to 0.8, were obtained in [23, 24, 28, 29]. The roughness indices—0.5 for small scales and 0.8 for large scales—were proposed by Bouchaud [22].

Spectra calculated for topographic profiles of faults have the functions of the spectral power density  $G(f)$  with an equation of the form  $G(\lambda) = C\lambda^{1+2\xi}$ , where  $C$  is the constant factor,  $\xi$  is the Hurst exponent or roughness index, and  $\lambda$  is the wavelength, i.e. the spectra can be described by a linear fractal model [19, 20]. At the same time, the study of fault profiles

parallel to slip and profiles normal to slip reveals the anisotropy of roughness [20, 26, 28, 30].

Recent experiments on rocks [31] confirmed that the ideas formulated for industrial materials [32] are valid for the microlevel: normal stress on contacting irregularities (termed asperities in seismology)  $\sigma_a$  can be roughly considered independent of the nominal normal stress  $\sigma_n$ :

$$\sigma_a \approx E \tan \theta, \quad (3)$$

where  $\theta$  is the local slope of asperities, and  $E$  is Young's modulus of the geomaterial.

In this case, there exists a certain critical angle  $\theta_c$ , such that peaks with  $\theta_1 > \theta_c$  and the above-average height for a given surface fail in shear, while peaks with  $\theta_2 < \theta_c$  are elastically deformed. For materials such as granite and gabbro, the critical angle ranges from 7° to 20° [31].

Under shear, asperities with supercritical angles are gradually destroyed. Thus, in a granite sample cut and polished to the grain size 600 grit at the normal stress from 10.2 to 14.3 MPa, the number of asperities with  $\theta > 17^\circ$  amounts to  $\sim 54 \pm 16\%$  before shear and to  $25 \pm 15\%$  after shear [31].

After shear, the fault surfaces become noticeably smoother as compared to the profiles measured before slip, thus giving a less steep roughness spectrum. For example, the slope angles  $\beta = 2.3 \pm 0.1$  in the spectrum before slip and  $\beta = 1.4 \pm 0.4$  after slip were experimentally measured [31]. A similar decrease in the initial slope from  $\beta > 2$  (without shear) to  $\beta < 2$  (after shear) for a profile parallel to the slip direction was found by profilometry of fracture surfaces moved tens to hundreds of meters.

At large displacement amplitudes, wear products fill the main fault, thus forming the fault gouge. The central fault zone can include one or several main faults and is surrounded by a damage zone (a zone of increased crack density as compared to the host rock). The damage zone is believed to be caused by the change in the slip zone geometry when the fault abruptly changes the direction of propagation, shear displacement predominantly in weaker interlayers within the fault zone, and concentration of stresses exceeding the rock strength in the vicinity of the main fault [27].

At the initial stages of faulting, when the surface roughness is still high and the displacement of the sides is relatively small, the damage zone width is close in magnitude to the shear amplitude. The average asperity amplitude on the walls of tectonic cracks (shear, tensile, and cooling ones), if not crossing rock strata, is usually less than one percent of the

crack length [5]. At large shear amplitudes (more than several percent of the length), the damage zone width becomes, in accordance with (2), proportional to  $L^{0.8}$  and almost independent of the shear amplitude. This means that at high displacement amplitudes in the mature fault zones, their width increases much more slowly than at small displacements. Since the fault length is thought to correlate with the shear amplitude [33], a boundary was found between faults with different scale ratios. The boundary is marked by the fault length  $L \sim 500\text{--}1000$  m, above which the fault is called mature [25, 27, etc.]. Analysis of the available research data on the fault zone width also leads to the conclusion that scale ratios vary in transition to the mature fault zones [27].

Thus, at a certain stage of the fault evolution, the rate of growth of the fault width is significantly slowed down: all asperities above a certain height become destroyed and the remaining asperities on the slip surface play the role of stress concentrators. These stress concentration zones are surrounded by large unloaded zones, whose area is approximately two orders of magnitude larger than the contact area [5].

Another process can develop in subduction zones, where asperities of the sinking plate, the so-called seamounts, can be so large (up to several kilometers in height) that they have a significant effect on the slip process. For example, the southern part of the 2011 Tohoku earthquake rupture was arrested just in the seamount subduction zone [34]. Such cases are beyond the scope of this work.

### 3. SLIP LOCALIZATION

One of the important achievements of the last 25 years in fault geomechanics was the establishment of the fact that shear on seismogenic rupture inside the fault core is highly localized. The results of a geological description of fault regions lifted during evolution from great depths, data from fault drilling, detailed studies of the position of well defined foci of microseismic events show that macroscopic block displacements are not distributed throughout the rock previously fractured by shear, but localize along a narrow slip surface. The roughness of this surface is one of the parameters characterizing the central fault zone, where the slip process is chiefly localized. High-amplitude shear displacements often occur in the fault core within ultracataclastic, clay-bearing zones tens to hundreds of millimeters thick, but the main coseismic shear can be localized in a 1–5-mm-thick zone of the ultracataclasite core [35].

For example, according to [36], out of 10 km of shear displacement in a section of the Punchbowl fault, only 100 m are localized in the damage zone about 100 m thick, and the rest displacement took place in a narrow ultracataclasite core. This ultracataclasite layer from 4 cm to 1 m in thickness includes a rather flat continuous surface, which serves as the principal fracture surface during the last several kilometers set in motion. The principal fracture surface is an ultracataclasite layer about 1 mm thick [37].

Individual zones of the principal fracture surface can rarely be traced for more than several hundred meters, although it is assumed that their length can reach many kilometers [38]. It is quite probable that at certain deformation stages the principal fracture surfaces can interact through distributed cataclastic strain zones without clear traces of a single rupture [27].

The coalescence of echelon cracks into the system was demonstrated in the previous numerical experiment [27]. The calculation results show that the width of the block displacement localization is orders of magnitude smaller than the thickness of the material crushed in shear.

Thus, the results of studying the slip surface geometry and regularities of shear localization allowed a number of authors to propose an elaborate phenomenological model of formation of the central zone of a seismogenic fault [21, 39, 40].

The main stages of the fault evolution are shown in Fig. 1. At the stage of the protocrack propagation, a discontinuity appears in the host rock, with the damage zone containing cracks of a lower hierarchical level around it. At the initial stage of evolution, an immature fault presents the close contact of rock surfaces (Fig. 1a) with fractured zones (Fig. 1b). As noted above, with strain accumulation, the effective width of the fractured zones increases almost proportionally to the shear amplitude (Fig. 1c). At low displacement velocities and amplitudes, the process of hydrothermal healing becomes competitive, resulting in the healed zone. With further relative displacement, the gouge layer reaches a critical thickness, so that the central zone width almost ceases to increase (Fig. 1d), and the effective fault strength and wear rate noticeably decrease. Since a comminuted material is highly reactive, the gouge layer may harden with time under high pressure and temperature, for example, due to dehydration or agglomeration (Fig. 1e). An increase in the stiffness of the central zone, as will be shown below, can result in instability

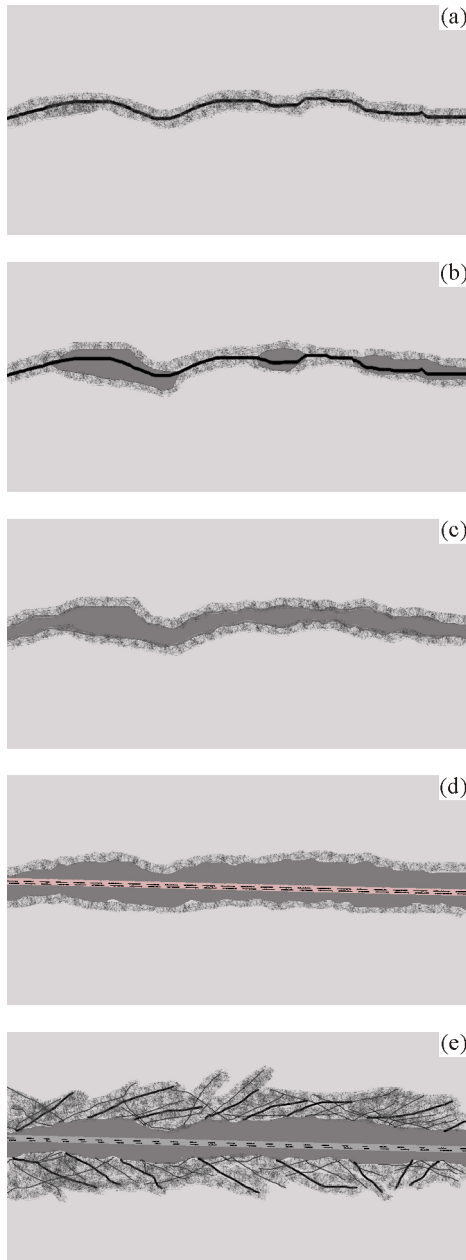


**Fig. 1.** Stages of formation of the central part of the seismogenic fault.

of dynamic slip and secondary rupturing. The most important role belongs here to features of rock friction.

#### 4. FRICTION

A common assumption in the mechanics of faults and earthquakes is that earthquakes originate in mechanically strong fault regions (irregularities), while aseismic slip occurs in weak regions (for example, [41, 42]). However, numerous studies carried out in the last two decades convincingly demonstrate that

the regularities of initiation and propagation of an earthquake rupture are determined by the frictional interaction of fault sides along the localized slip surface. The conditions for dynamically unstable slip are well studied. In the stick-slip model, the source parameters and the onset of instability are independent of absolute contact strength, but is determined by relative changes in frictional strength  $\tau_{fr}$ .

A necessary condition for slip is a decrease in  $\tau_{fr}$  with increasing slip velocity  $v$  and/or displacement amplitude  $D$ , the so-called velocity weakening:

$$\frac{d\tau_{fr}}{dv} < 0, \frac{d\tau_{fr}}{dD} < 0. \quad (4)$$

In addition, as in Griffiths crack mechanics, the initiation and arrest conditions are determined by the relation of the rate of dynamic release of elastic strain energy  $K$  to the rate of absorption of crack propagation energy  $k_s$ . In frictional sliding, the first parameter is the rate at which the stress can be elastically unloaded in the host material with the elastic modulus  $G$ :  $K = \eta G / \hat{L}$ , and the second parameter  $|k_s| = |\partial\tau / \partial D|$  is the rate at which friction changes with cumulative displacement  $D$  with growing slip velocity. In these expressions,  $G$  is the shear modulus of the host rock,  $\eta \sim 1$  is the form factor,  $\hat{L}$  is the characteristic size associated with the earthquake magnitude [27].

Given the condition  $\psi = |k_s| / K > 1$ , the energy is radiated from the system. Otherwise dynamic slip and consequently energy radiation are impossible. The ratio determines not only the possibility, but also the pattern of slip. This issue was studied in a series of publications [43–45]. Figure 2 shows the dependence of the shear force drop during a slip event on the content of clay in the quartz sand mixture filling the contact between the rigid blocks. The experiment is detailed in [43, 45]. It is clearly seen that with increasing content of clay particles (decreasing contact stiffness), the stress drop amplitude in the rock and consequently the radiated energy decrease by several orders of magnitude. In this case, the frictional strength of the contact remains almost unchanged [45].

According to [45], slow slip regimes occur in the narrow range  $\psi \sim 1 \div 2$ , while stick slip allows for a wider variation in this parameter. Since the crustal rock rigidity varies slightly for different regions and different depths, the fault stiffness  $k_s$  acts as a control parameter. On brittle faults, where the stiffness (the rate of decrease in shear resistance) is high enough,

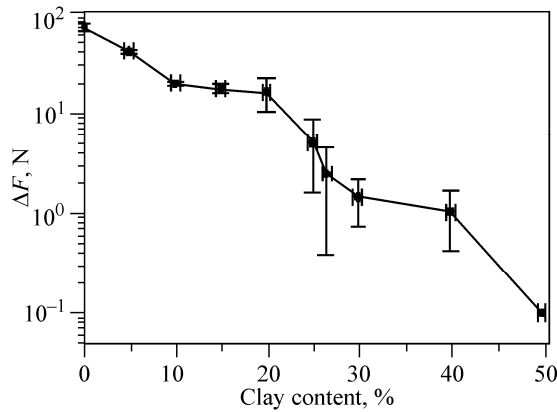


**Fig. 2.** Shear force drop during a slip versus the clay content in the gouge. The loading stiffness  $K = 28$  N/mm.

the strain energy is realized only in the form of dynamic slips, i.e. “normal” earthquakes. Slow slip events can occur on faults with low stiffness.

In view of highly localized shear, the described macroscopic effects are determined by processes occurring at the meso- and microlevels.

Within the rate-and-state friction law, which is commonly used to describe frictional slip on faults [46, 47], the type of the dependence of friction on the slip velocity is described by the so-called frictional parameter

$$a - b = \frac{\Delta\mu}{\ln(V/V_0)}, \quad (5)$$

where  $\Delta\mu$  is the friction coefficient variation with slip velocity increasing from  $V_0$  to  $V$  [46]. Positive values ( $a - b$ ) indicate that the material has the property of velocity strengthening, and at  $a - b < 0$  the material has the property of velocity weakening. The empirical nature of the rate-and-state friction laws is an obvious disadvantage, limiting this model to natural objects. In recent years, significant steps have been taken to elucidate the physical nature of friction variations in the fault gouge under different pressure–temperature conditions.

Both the fault stiffness and the parameter ( $a - b$ ) depend on the material composition of the slip zone, water content, chemical composition of the fluid, and pressure–temperature conditions. These characteristics are most sensitive to the material composition in the slip zone. For example, the presence of watered clays (or of talc, which often replaces minerals of the serpentine group along the fracture walls when serpentine reacts with silicon dioxide contained in thermal fluids) dramatically reduces the fault shear stiffness, up to 10% of the normal value. Some fault

segments at seismogenic depths can have significantly decreased stiffness due to sublithostatic pore-fluid pressure. According to Rice [48], it can be observed in isolated layers in the central part of the fault, which are bounded by low-permeability formations.

Over the last 10 years, several laboratories have investigated the influence of particle-related properties on the macroscopic slip laws [26, 29, 49–51, etc.].

Many gouges in the fault slip zone have the frictional strength typical of geomaterials (the friction coefficient for stable slip at low velocity is  $\mu_0 \sim 0.6$ ), but some gouges rich in phyllosilicates (silicates with a layered structure, such as micas, chlorites, etc.) are much weaker ( $\mu_0$  is just about 0.2–0.3) [50].

Chen et al. [26] studied the dependence of the friction coefficient  $\mu_0$  on the surface roughness for some materials and came to an important result. On the asperity scale  $\sim 0.01$ – $10$   $\mu\text{m}$ , friction coefficients strongly correlate with roughness. With increasing microroughness, the  $\mu_0$  values rather quickly rise to  $\sim 0.65$ – $0.80$ , which corresponds to the universal Beyrlee’s law for macroscopic friction of rock surfaces [16]. This led the authors to the conclusion that the decrease in friction on faults is primarily controlled by wear (decrease in roughness) on the scale 0.01– $10$   $\mu\text{m}$ , while roughness on large scales of natural faults has a limited effect on the  $\mu_0$  value [27].

The study of the frictional parameter ( $a - b$ ) for various gouges (see, for example, [50]) clearly demonstrated that the frictional behavior of these materials depends on their basic friction coefficient  $\mu_0$  (Fig. 3). Gouges with the lowest friction coefficients (talc, montmorillonite, biotite, muscovite, etc.) exhibit the property of velocity strengthening under any conditions,  $a - b > 0$  (Fig. 4a). For example, a material such as saponite, which has a low friction coef-

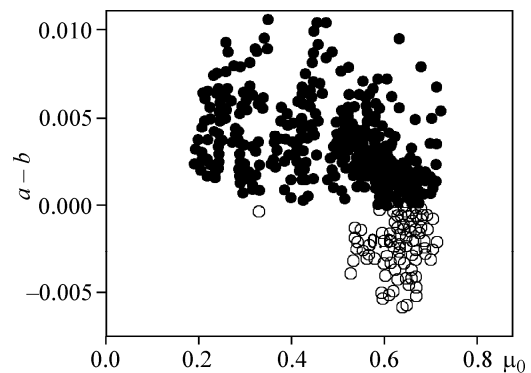


**Fig. 3.** Frictional parameter  $a - b$  versus friction coefficient  $\mu_0$  (according to [50]).

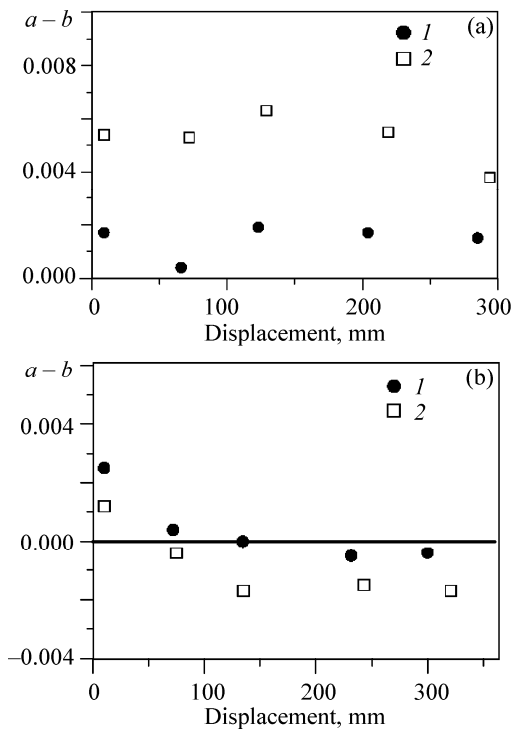


**Fig. 4.** Frictional parameter  $a-b$  versus shear amplitude: chlorite,  $\sigma_n = 20$  MPa (a), Westerly granite,  $\sigma_n = 50$  MPa (b); displacement velocity 1–3 (1) and 30–100  $\mu\text{m/s}$  (2) (according to [50]).

ficient increasing with slip velocity, determines the deformation behavior of the creeping section of the San Andreas fault [52].

Gouges containing materials with high friction coefficients (quartz, feldspar, kaolinite, etc.) demonstrate, depending on the pressure–temperature conditions, loading rate, and shear amplitude, both velocity strengthening and weakening (Fig. 4b). It is noted that at higher basic friction coefficient  $\mu_0$ , both parameters  $a$  and  $b$  grow, but the latter has a faster growth, which leads to negative values of  $(a-b)$ , i.e. to the effect of velocity weakening [51]. Natural materials showing only frictional weakening with slip velocity have not yet been found.

Grain-related properties of microcontacts also determine the ability of the fault to recover strength with time. Various healing mechanisms of different-scale faults were analyzed in the previous paper. It was shown that complete recovery of strength properties of the material in the rupture zone (metamorphogenic healing) exerts no effect on the earthquake preparation, since the characteristic time of deep transformation of the material is too long. According to Ruzhich et al. [53], the empirical depend-

ence of the duration of fault healing on the fault length:

$$\log t \text{ (year)} = 1.53 \log L \text{ (m)} - 1.68, \quad (6)$$

which is several orders of magnitude higher than the earthquake preparation time of the corresponding magnitude [27].

At the same time, the adhesive and hydrothermal mechanisms are quite effective. According to the results of laboratory experiments, the rate of recovery of the contact shear strength after slip strongly depends on the effective asperity contact area [51] and effective porosity [54].

The increase in pressure and temperature gives rise to certain mechanisms that contribute to the contact strengthening with time. One of the important mechanisms is the dissolution of minerals in zones of increased normal stresses with subsequent rapid precipitation in relatively unloaded zones, the so-called compressive creep during dissolution [55]. This mechanism can lead to a rapid increase in both the contact area and the adhesion [56, 57].

The microstructural study disclosed that the strength recovery mechanism is associated with cohesive strengthening, cementation, and compaction of the fractured material, as well as with the microcrack filling in the fracture zone [54, 58]. The phyllosilicate contact is strengthened by transformation of hydrophilic clay minerals into hydrophobic micas [59]. An increase in the content of neutral quartz due to the separation of silica during the clay transformation [59] can also stimulate this effect. Phyllosilicate minerals are expected to have the form of highly layered mica or chlorite schists at elevated pressures and temperatures [59].

At higher temperatures and pressures corresponding to the lower seismogenic boundary, the rock becomes so plastic that the true contact area attains the saturation controlled by the crystal structure of a mineral. This actually means that the contact area does not change during shear, making weakening impossible. Some experiments that demonstrate frictional strengthening with slip velocity reveal a high gouge compaction, up to almost complete loss of porosity [60].

Thus, the localization of dynamic fault slip within the narrow ultracataclasite core, even during large earthquakes, points to a surprising, at first glance, fact: slip features on faults hundreds of kilometers long are determined almost exclusively by the properties of the contact between particles units, dozens, and hundreds of micrometers in size.

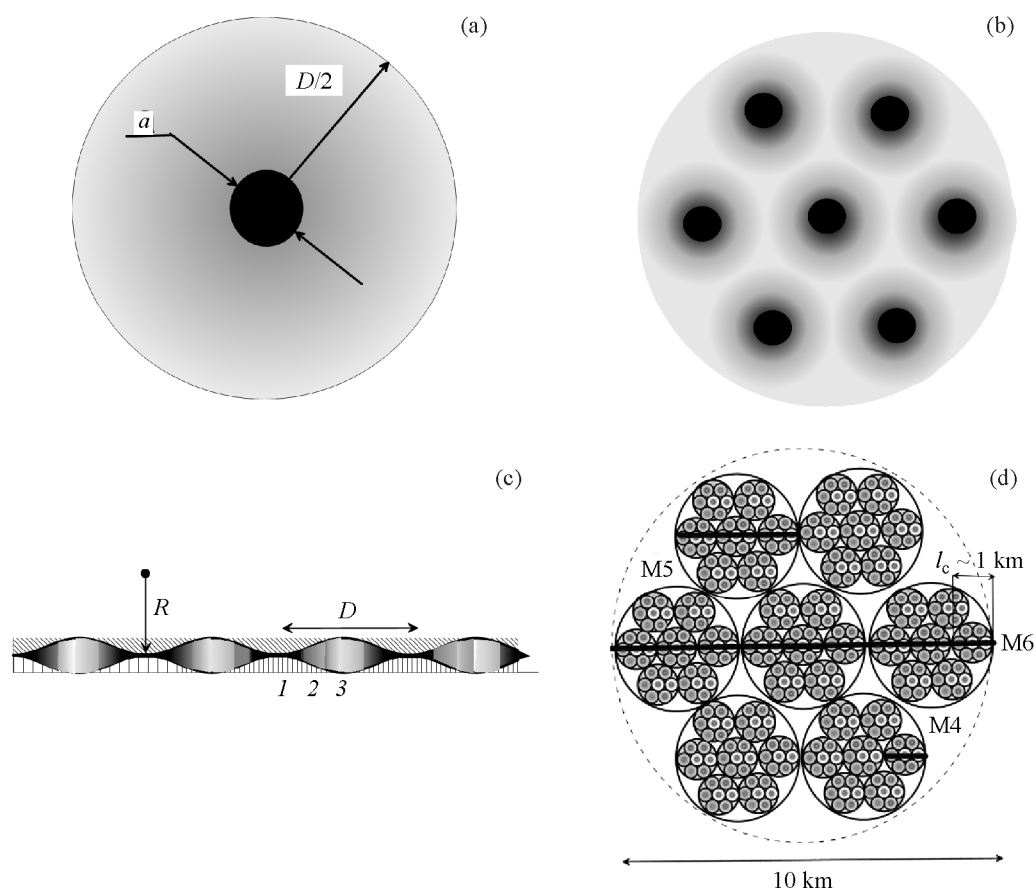


**Fig. 5.** The simplest model of the asperity contact: the true contact zone (stress concentration zone) with diameter  $a$  is surrounded by the unloaded zone with diameter  $D$  (a); plan view of a contact surface section (b); sectional view of the contact zone (c): velocity weakening zone (1), transient zone (2), velocity strengthening zone (3); idealized plane model of the contact surface section (d). Stress concentration zones (velocity weakening zones) are surrounded by unloaded zones. The line segments show rupture lengths of earthquakes of various magnitudes (M4, M5, and M6).

## 5. HIERARCHY OF REGIONS WITH DIFFERENT FRICTIONAL PROPERTIES

The complex topography of the slip surface leads, as noted above, to the appearance of the zones of stress concentration and relative unloading. Minerals transferred by fluids are precipitated in the unloaded zones, which contributes to the formation of interlayers of weak materials rich in phyllosilicates, i.e. surface regions with the frictional properties of velocity strengthening.

The stress concentration zones contain regions of strong gouge, being composed mainly of quartz and feldspar, i.e. initially almost free of phyllosilicates. The degree of shear localization grows on account of higher stress. All this significantly enhances the probability of the stick-slip regime.

Thus, it is these asperity contacts (stress concentration zones) that turn out to be dynamically unstable in fault slip, while the regions between the con-

tacting asperities are characterized by the frictional properties of stable slip.

The simplest frictional model of the asperity contact is shown in Fig. 5. The contact consists of loaded and unloaded regions. Stress concentration zones 1 will be taken as zones with the property of velocity weakening, maximum unloading zones 3 are, on the contrary, zones of increasing shear friction coefficient. Between these zones there is transition zone 2, in which the material does not have a pronounced dependence of friction on velocity and displacement.

In the first approximation, the size of the contact spot (weakening zone) can be estimated from the solution of the elastic Hertz problem [61, 62] (lower bound):  $a \approx \pi \sigma_n R / E$ , where  $R$  is the asperity curvature radius,  $a$  is the contact spot diameter,  $E$  is the modulus of elasticity, and  $\sigma_n$  is the normal stress. Then, at  $E = 10^{11}$  Pa and  $\sigma_n = 3 \times 10^8$  Pa, we derive  $a \approx 10^9 R / 10^{11} = 0.01R$ .



As noted above for laboratory samples, asperities have the critical angle  $\theta_c \sim 7^\circ \div 20^\circ$ , and larger slope angles cause their destruction during faulting. Taking into account a decrease in this value on a larger scale, we agree on the estimate of the angle of large-scale asperities on the fault surface [5]:  $\alpha \sim 5^\circ \div 10^\circ$ , whence it follows  $R = 0.5D/\sin(5^\circ \div 10^\circ) \approx (6 \div 12)D$ , or  $a \approx 0.01D$ .

Similarly to the hierarchy of blocks and stress concentration zones, strengthening and weakening zones also obey the hierarchical law. Zones of smaller contacts form a cluster, taken as an asperity of the next hierarchical level. If the dimension ratio of the neighboring hierarchical levels conforms to the Sadovsky hierarchical block model [3]  $L_{j+1}/L_j \sim 3$ , then, in the case of “close packing” in the 2D case, 7 contacts of level  $j$  form a cluster, which is an asperity of level  $j + 1$  (Fig. 5d). The Sadovsky hierarchical levels roughly correspond to a change in seismic magnitude by 1.

It is clear that what we have in reality is irregular distribution of surface asperities and gouges with properties determined by many factors apart from stresses. In this regard, the zones of strengthening and weakening can have different size. Large regions composed of slip-strengthened materials can be an insurmountable obstacle to dynamic rupture.

The results of numerical simulation of relative shear displacement of two elastic blocks with the slip surface between them are given in [63]. If the boundary condition is set at the contact, friction is described using the rate-and-state law [46]. In so doing, the slip plane has one or more spots where the model coefficients ensure the velocity weakening regime. On the rest slip surface, the friction force either is independent of the velocity and displacement, or meets the same rate-and-state law but with constants providing the velocity strengthening regime. In the calculations, controlled parameters are kinematic parameters of motion, stress tensor components, the spatial distribution of variation in shear energy density of the blocks and the kinetic energy at different time instants relative to the slip time.

Figure 6 presents the results for the calculation variant with four weakening spots. The rupture begins at one of these spots and propagates on either side of it. Outside the weakening zone, the displacement velocity rapidly decreases, again increasing at the adjacent spots. Although the maximum slip velocity rapidly decreases outside the weakening zone, the total relative displacement of the fault sides (the sum of dynamic displacement and slow preseismic

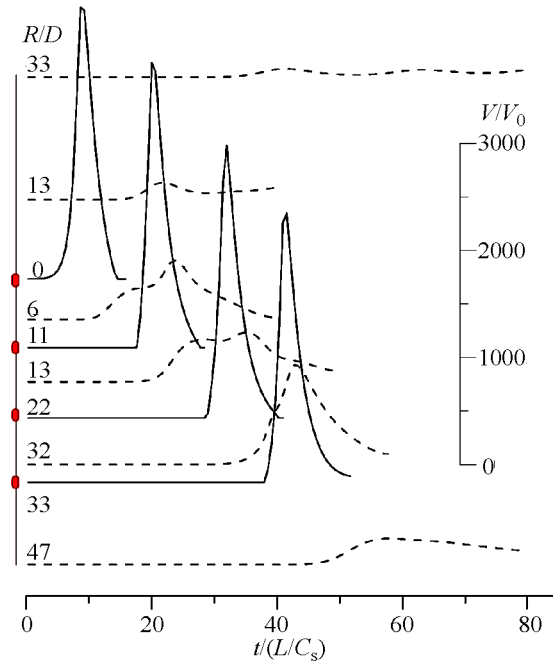


**Fig. 6.** Diagrams of the material displacement velocity in the direction parallel to the slip surface in the calculation variant with four identical zones of velocity weakening. The location of the zones/spots is shown in bold segments on the left axis. Coulomb friction is set outside the spots. Distance from the point of a rupture normalized to the spot diameter  $D$  is marked above the curves. Solid lines are plotted for points inside the spots; dotted lines, for points outside the spots. The mass velocity amplitude is normalized to the displacement velocity of the block edge. For the sake of readability, only the first phases of displacement are shown in the figure.

and postseismic slips) remains almost unchanged. In this case, the higher the total fraction of weakening zones, the higher the fraction of strain energy spent on the elastic wave radiation in the high-frequency spectrum portion [63].

According to the calculation results, the rupture propagates along the stressed tectonic fault up to the contact spot with velocity-strengthening property, where the displacement velocity decreases rapidly. If the strengthening zone is large enough, the rupture is arrested. If the strengthening zone is small, the rupture slips it, accelerating again at weakening spots.

## 6. OBSERVATION OF EQRTHQAKE RUPTURES

Clusterization, in analogy with the above-described simple model, can be observed in respect to the location of sources of the so-called repeated earthquakes, i.e. events of close magnitude, which occur almost in the same place at different times. A

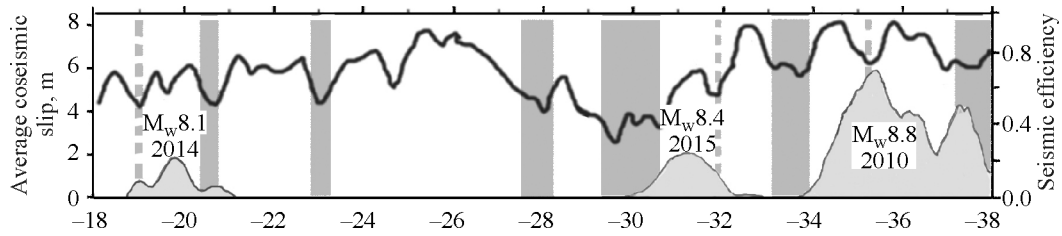


**Fig. 7.** Distribution of seismic efficiency according to [66]. The upper curve is the distribution of seismic efficiency depending on the latitude of the Chilean subduction zone (the right ordinate). Grey vertical portions correspond to regions of low seismic efficiency. Lower curves are the distribution of coseismic slip during the three largest earthquakes (the left ordinate).

coincident location of the sources points to the fact that repeated earthquakes most probably rupture the same region of the fault, i.e. asperity. This idea is also confirmed by the almost identical form of the seismograms recorded from different events of the same multiplet by the same station. We reproduced such events in a laboratory experiment [64].

Repeated events are quite common. Among 7409 events registered over 15 years of observations at the Calaveras fault, 4890 (66%) had at least one repeated event within the 25-m distance. Repeated earthquakes are detected both in the background seismicity and in the aftershock sequence of larger events throughout the world [65].

The location of a source and the size of a rupture due to repeated earthquakes are determined to very high accuracy, so that their analysis can give a good estimate of the asperity size in the source of small seismic events.

Data on asperities can also be derived from geodetic monitoring. According to the results of GPS measurements, the seismic efficiency coefficient  $\chi$ , or seismic cohesion, is determined as

$$\chi = \frac{\dot{P}_s}{v_p S_f}, P_s = \frac{M_0}{G} = \int_S u dS, \quad (7)$$

where  $M_0$  is the seismic moment,  $G$  is the shear modulus,  $u$  is the vector of coseismic displacement,  $S_f$  is the rupture area, and  $v_p$  is the velocity of displacement of the plate under tectonic forces.

It is assumed that in the asperity region, where the fault is locked in the interseismic period,  $\chi = 1$ , i.e. the displacement is gained due to coseismic slip. In the surrounding region, slip is conditionally stable (slip is stable under a quasi-static load, but it can become unstable under a dynamic load above a certain value), and the seismic efficiency coefficient is  $0 < \chi < 1$ . In creep regions without large earthquakes, the coefficient  $\chi$  is small.

For obvious reasons, such measurements are informative mainly in subduction zones, where plate

displacement velocities are high enough and large earthquakes occur.

Figure 7 exemplifies the distribution of seismic efficiency (upper lines) depending on the latitude of the Chilean subduction zone. It also shows the distribution of the coseismic slip (bottom line) during the three largest earthquakes. The gray vertical portions correspond to regions of low seismic efficiency, bounding the locked regions. It is clearly seen that the rupture hardly propagates into the regions of low cohesion (presumably the regions with the dominant frictional properties of velocity strengthening).

Judging from the rupture location of the large paleoearthquakes along the Chilean subduction zone [66], we constructed the total density of rupture length along the strike of the subduction zone. As can be seen from the diagram, the zones of maximum density of rupturing approximate the distribution of GPS-measured seismic efficiency (Fig. 8), and the characteristic dimensions of asperities of mega earthquakes with  $M_w > 8$  are 100–200 km. In so doing, the  $M_w = 8.8$  Maule earthquake rupture includes two such regions.

It is currently difficult to reliably measure dimensions of asperities as physical objects, i.e. regions

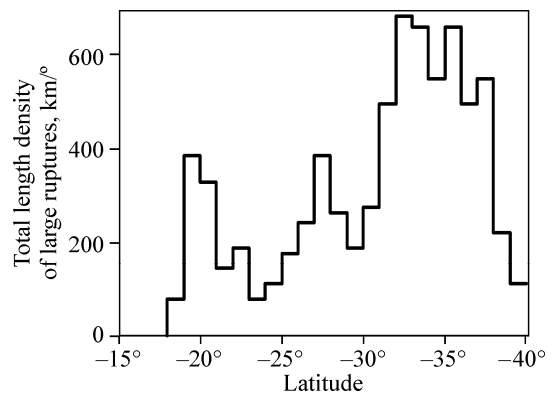


**Fig. 8.** Total density of rupture length of large earthquakes (1615–2015) along the strike of the Chilean subduction zone.

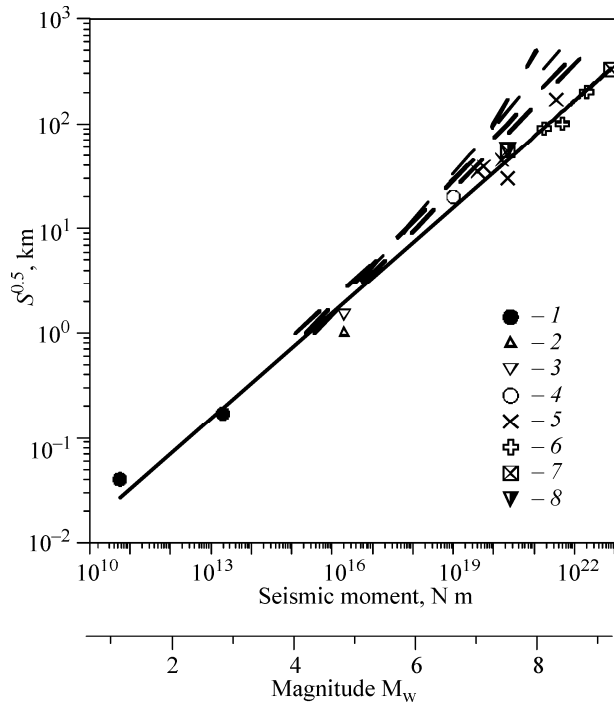


**Fig. 9.** Average size of asperities versus the earthquake scale.  $S$  is the effective area of asperities. 1—[67], 2—[68], 3—[69], 4—[70], 5—[71], 6—[66], 7—[72], 8—[73].

with certain frictional characteristics. The problem is that the size analysis of maximum slip amplitude zones and the data on seismic efficiency coefficient are not enough to establish the boundary between the frictional weakening zone (true asperity) and conditionally stable zones to which a rupture can propagate at a rather high slip velocity.

Figure 9 summarizes the published data on the characteristic dimensions of asperities depending on the earthquake. Despite the fact that this information refers to different regions, and asperities are identified from different evidence, the data set with the determination coefficient  $R=0.986$  is described by the ratio

$$\sqrt{S} = 6.33 \times 10^{-6} M_0^{0.34}, \quad (8)$$

where  $S$  is the asperity area in  $\text{km}^2$ , and  $M_0$  is the seismic moment of an earthquake in  $\text{N m}$ . The exponent in relation (8) corresponds to the geometric similarity, which is usually found in seismic characteristics in a wide range of magnitudes. The value  $S^{0.5}$  is quite close to the empirical dependences used to estimate the characteristic lengths of earthquake ruptures from the seismic moment, which are given in many works and summarized in monograph [27]. Some of them are shown in Fig. 9 with dashed lines.

It can be seen that the parameter  $S^{0.5}$  of the regions interpreted as asperities is, on average, 1.5–3 times less than the rupture length. Apparently, the weakening zones should still be noticeably smaller. The size of these zones can be more reliably determined through a thorough analysis of high-frequency records around the source, revealing their fine structure.

### 7. CONCLUSIONS

The brief review performed for the concepts and recent results on fault slip focuses mainly on the analysis of the hierarchy of structures that form the slip zone of a seismogenic fault and on their relation to mechanical characteristics that determine the dynamics of macroscopic deformation in the fault zone.

The influence of the microparticle contact properties in the shear localization zone on the slip behavior of faults hundreds of kilometers long was revealed. This influence is realized through consistent interaction within a multilevel hierarchical system.

The interaction of asperities at the initial stage of the protocrack shear forms a layer of comminuted material, which, due to fluids and in the crustal pressure–temperature conditions, acquires properties that determine the frictional characteristics of the fault faces in the slip zone. These characteristics turn out to be responsible for the slip regime: stable creep, slow slip events or dynamic slip resulting in an earthquake. Careful extrapolation of the laboratory data to nature leads to the assumption that a decrease in the fault friction is primarily controlled by wear (decreased roughness) on a scale of 0.01–10  $\mu\text{m}$ , while large-scale roughness on natural faults has a limited effect on the friction. Judging from the results obtained, the properties of microcontacts at the grain level determine not only the possibility of instability, but also the ability of a fault to recover strength with time.

Though being too simplified to claim an adequate description of natural processes, the considered scheme of the hierarchy of asperities in the fault zone reflects the important idea that the initiation, evolution, and arrest of a seismogenic rupture are determined by the presence of regions with different dynamics of frictional characteristics during slip: zones of weakening, strengthening, and almost neutral to velocity and displacement. A dynamic rupture always starts in the weakening zone (asperity). Based on the seismological data, the epicenter is often located at the periphery of the zone of maximum seismic efficiency. This issue has yet to be dealt with.

Between the weakening zones, the rupture velocity and slip velocity decrease, increasing again at the adjacent spots. In large strengthening zones, the earthquake degenerates into a slow slip event, or the rupture is completely arrested.

Observations during seismic events of different magnitudes show that even the largest earthquakes often rupture the same region of the crust. Unfortunately, the accuracy of observations and the usual ambiguity in the interpretation of the solution to the inverse problem do not yet allow a reliable identification of fault regions with velocity weakening. The analysis of the records of high-frequency oscillations in the vicinity of the fault can give more accurate results on the size and location of these zones. A good basis for the interpretation of such records can be found in the fundamental concepts of physical mesomechanics as the science of multilevel hierarchically organized systems.

#### FUNDING

The study was carried out with the financial support of the Russian Foundation for Basic Research within scientific project No. 20-55-53031.

#### REFERENCES

- Cailleus, A. and Tricart, J., Le problème de la Classification des Faits Géomorphologiques, *Annales de Géographie*, 1956, vol. 65, no. 349, pp. 162–186.
- Piotrovskii, V.V., Application of Morphometry to Studies of the Earth's Relief and Structure, in *The Earth in the Universe*, Fedynskii, Ed., Jerusalem: Israel Program for Scientific Translations, 1968, pp. 228–243.
- Sadovsky, M.A., Bolkhovitinov, L.G., and Pisarenko, V.F., *Deformation of the Geophysical Medium and Seismic Process*, Moscow: Nauka, 1987.
- Rodionov, V.N., Sizov, I.A., and Tsvetkov, V.M., *Fundamentals of Geomechanics*, Moscow: Nedra, 1986.
- Kocharyan, G.G. and Spivak, A.A., *Dynamics of Rock Deformation*, Moscow: Akademkniga, 2003.
- Panin, V.E., Foundations of Physical Mesomechanics, *Phys. Mesomech.*, 1998, vol. 1, no. 1, pp. 5–20.
- Panin, V.E., Egorushkin, V.E., and Panin, A.V., Physical Mesomechanics of a Deformed Solid as a Multilevel System. I. Physical Fundamentals of the Multilevel Approach, *Phys. Mesomech.*, 2006, vol. 9, no. 3–4, pp. 9–20.
- Panin, V.E. and Egorushkin, V.E., Deformable Solid as a Nonlinear Hierarchically Organized System, *Phys. Mesomech.*, 2011, vol. 14, no. 5–6, pp. 207–223.
- Panin, V.E., Fomin, V.M., and Titov, V.M., Physical Principles of Mesomechanics of Surface Layers and Internal Interfaces in a Solid under Deformation, *Phys. Mesomech.*, 2003, vol. 6, no. 3, pp. 5–13.
- Scholz, C.H., Paradigms or Small Change in Earthquake Mechanics, in *Fault Mechanics and Transport Properties of Rocks*, Evans, B. and Wang, T., Eds., Academic Press Limited, 1992, pp. 505–517.
- Chinnery, M.A., The Strength of the Earth's Crust under Horizontal Shear Stress, *J. Geophys. Res.*, 1964, vol. 69, pp. 2085–2089.
- Brace, W.F. and Byerlee, J.D., Stick-Slip as a Mechanism for Earthquakes, *Science*, 1966, vol. 153, pp. 990–992.
- Kanamori, H. and Stewart, G.S., Seismological Aspects of the Guatemala Earthquake of February 4, 1976, *J. Geophys. Res.*, 1978, vol. 83, pp. 3427–3434.
- Ruzhich, V.V. and Kocharyan, G.G., On the Structure and Formation of Earthquake Sources in the Faults Located in the Subsurface and Deep Levels of the Crust. I. Subsurface Level, *Geodin. Tektonofiz.*, 2017, vol. 8, no. 4, pp. 1021–1034. <https://doi.org/10.5800/GT-2017-8-4-0330>
- Rebetsky, Yu.L., Regularities of Crustal Faulting and Tectonophysical Indicators of Fault Metastability, *Geodin. Tektonofiz.*, 2018, vol. 9, no. 3, pp. 629–652. <https://doi.org/10.5800/GT-2018-9-3-0365>
- Byerlee, J.D., Friction of Rocks, *Pure. Appl. Geophys.*, 1978, vol. 116, pp. 615–626.
- Scholz, C.H., *The Mechanics of Earthquakes and Faulting*, Cambridge: Cambridge University Press, 2002.
- Marone, C., Laboratory Derived Friction Laws and Their Application to Seismic Faulting, *Ann. Rev. Earth Planet. Sci.*, 1998, vol. 26, pp. 643–696.
- Mandelbrot, B., *The Fractal Geometry of Nature*, San Francisco: Freeman, 1982.
- Power, W.L., Tullis, T.E., Brown, S.R., Boitnott, G.N., and Scholz, C.H., Roughness of Natural Fault Surfaces, *Geophys. Res. Lett.*, 1987, vol. 14, pp. 29–32.
- Kocharyan, G.G. and Kulyukin, A.M., Study of Caving Features for Underground Workings in a Rock Mass of Block Structure with Dynamic Action. Part II. Mechanical Properties of Interblock Gaps, *J. Mining Sci.*, 1994, vol. 30, no. 5, pp. 437–446. <https://doi.org/10.1007/BF02047334>
- Bouchaud, E., Scaling Properties of Cracks, *J. Phys. Condens. Matter.*, 1997, vol. 9, pp. 4319–4344.
- Sagy, A. and Brodsky, E.E., Geometric and Rheological Asperities in an Exposed Fault Zone, *J. Geophys. Res. B*, 2009, vol. 114, p. 02301. <https://doi.org/10.1029/2008JB005701>
- Amitrano, D. and Schmittbuhl, J., Fracture Roughness and Gouge Distribution of a Granite Shear Band, *J. Geophys. Res. B*, 2002, vol. 107, no. 12, p. 2375. <https://doi.org/10.1029/2002JB001761>
- Brodsky, E.E., Kirkpatrick, J.D., and Candela, T., Constraints from Fault Roughness on the Scale-

- Dependent Strength of Rocks, *Geology*, 2016, vol. 44, no. 1, pp. 19–22. <https://doi.org/10.1130/G37206.1>
26. Chen, X., Madden, A.S., Bickmore, B.R., and Reches, Z., Dynamic Weakening by Nanoscale Smoothing during High-Velocity Fault Slip, *Geology*, 2013, vol. 41, no. 7, pp. 739–742. <https://doi.org/10.1130/G34169.1>
  27. Kocharyan, G.G., *Geomechanics of Faults*, Moscow: GEOS, 2016.
  28. Candela, T., Renard, F., Bouchon, M., Schmittbuhl, J., and Brodsky, E.E., Stress Drop during Earthquakes: Effect of Fault Roughness Scaling, *Bull. Seismol. Soc. Am.*, 2011, vol. 101, no. 5, pp. 2369–2387. <https://doi.org/10.1785/0120100298>
  29. Selvadurai, P.A. and Glaser, S.D., Asperity Generation and Its Relationship to Seismicity on a Planar Fault: A Laboratory Simulation, *Geophys. J. Int.*, 2017, vol. 208, pp. 1009–1025.
  30. Sagy, A., Brodsky, E.E., and Axen, G.J., Evolution of Fault-Surface Roughness with Slip, *Geology*, 2007, vol. 35, pp. 283–286. <https://doi.org/10.1130/G23235A.1>
  31. Chen, X., Carpenter, B.M., and Reches, Z., Asperity Failure Control of Stick–Slip along Brittle Faults, *Pure Appl. Geophys.*, 2020, vol. 177, pp. 3225–3242. <https://doi.org/10.1007/s00024-020-02434-y>
  32. Tabor, D., Interaction between Surfaces: Adhesion and Friction, in *Surface Physics of Materials*, Blakeley, J.M., Ed., Ch. 10, New York: Academic Press, 1975.
  33. Ruzhich, V.V. and Sherman, S.I., Estimation of the Relation between the Length and Amplitude of Fault Displacements, in *Crustal Dynamics in Eastern Siberia*, Novosibirsk: Nauka, 1978, pp. 52–57.
  34. Wang, K. and Bilek, S.L., Fault Creep Caused by Subduction of Rough Seafloor Relief, *Tectonophysics*, 2014, vol. 610, pp. 1–24.
  35. Rice, J.R., Heating and Weakening of Faults during Earthquake Slip, *J. Geophys. Res. B*, 2006, vol. 111, no. 5, p. 05311. <https://doi.org/10.1029/2005JB004006>
  36. Chester, F.M. and Chester, J.S., Ultracataclastic Structure and Friction Processes of the Punchbowl Fault, San Andreas System, California, *Tectonophysics*, 1998, vol. 295, pp. 199–221.
  37. Chester, J.S., Chester, F.M., and Kronenberg, A.K., Fracture Surface Energy of the Punchbowl Fault, San Andreas System, *Nature*, 2005, vol. 437, pp. 133–136.
  38. Sibson, R.H., Thickness of the Seismic Slip Zone, *Bull. Seismol. Soc. Am.*, 2003, vol. 93, no. 3, pp. 1169–1178.
  39. Reches, Z. and Lockner, D.A., Fault Weakening and Earthquake Instability by Powder Lubrication, *Nature*, 2010, vol. 467, pp. 452–455. <https://doi.org/10.1038/nature09348.39>
  40. Boneh, Y. and Reches, Z., Geotribology—Friction, Wear, and Lubrication of Faults, *Tectonophysics*, 2018, vol. 733, pp. 171–181. <https://doi.org/10.1016/j.tecto.2017.11.022>
  41. Ruff, L. and Kanamori, H., Seismic Coupling and Uncoupling at Subduction Zones, *Tectonophysics*, 1983, vol. 99, no. 2–4, pp. 99–117. [https://doi.org/10.1016/0040-1951\(83\)90097-5](https://doi.org/10.1016/0040-1951(83)90097-5)
  42. Tichelaar, B.W. and Ruff, L.J., Depth of Seismic Coupling along Subduction Zones, *J. Geophys. Res. B*, 1993, vol. 98, no. 2, pp. 2017–2037. <https://doi.org/10.1029/92JB02045>
  43. Kocharyan, G.G. and Novikov, V.A., Experimental Study of Different Modes of Block Sliding along Interface. Part 1. Laboratory Experiments, *Phys. Mesomech.*, 2016, vol. 9, no. 2, pp. 189–199. <https://doi.org/10.1134/S1029959916020120>
  44. Budkov, A.M. and Kocharyan, G.G., Experimental Study of Different Modes of Block Sliding along Interface. Part 3. Numerical Modeling, *Phys. Mesomech.*, 2017, vol. 20, no. 2, pp. 203–208. <https://doi.org/10.1134/S1029959917020102>
  45. Kocharyan, G.G., Novikov, V.A., Ostapchuk, A.A., and Pavlov, D.V., A Study of Different Fault Slip Modes Governed by the Gouge Material Composition in Laboratory Experiments, *Geophys. J. Int.*, 2017, vol. 208, pp. 521–528. <https://doi.org/10.1093/gji/ggw409>
  46. Dieterich, J.H., Modeling of Rock Friction: 1. Experimental Results and Constitutive Equations, *J. Geophys. Res.*, 1979, vol. 84, pp. 2161–2168.
  47. Ruina, A.L., Slip Instability and State Variable Friction Laws, *J. Geophys. Res.*, 1983, vol. 88, pp. 10359–10370.
  48. Rice, J.R., Fault Stress States, Pore Pressure Distributions, and the Weakness of the San Andreas Fault, in *Fault Mechanics and Transport Properties of Rocks*, Evans, B. and Wong, T.-F., Eds., 1992, pp. 475–504.
  49. Reches, Z., Chen, X., and Carpenter, B., Asperity Failure Control of Stick-Slip along Brittle Faults, *Pure Appl. Geophys.*, 2020. <https://doi.org/10.1007/s00024-020-02434-y>
  50. Ikari, M.J., Marone, C., Saffer, D.M., and Kopf, A.J., Slip Weakening as a Mechanism for Slow Earthquakes, *Nature Geosci.*, 2013, vol. 6, pp. 468–472. <https://doi.org/10.1038/NNGEO18198>
  51. Carpenter, B.M., Ikari, M.J., and Marone, C., Laboratory Observations of Time-Dependent Frictional Strengthening and Stress Relaxation in Natural and Synthetic Fault Gouges, *J. Geophys. Res. Solid Earth.*, 2016, vol. 121, pp. 1183–1201. <https://doi.org/10.1002/2015JB012136>
  52. Scholz, C.H. and Campos, J., The Seismic Coupling of Subduction Zones Revisited, *J. Geophys. Res. B*, 2012, vol. 117, p. 05310. <https://doi.org/10.1029/2011JB009003>
  53. Ruzhich, V.V., Medvedev, V.Ya., and Ivanova, L.A., Healing of Seismogenic Ruptures and Earthquake Re-

- currence, in *Seismicity of the Baikal Rift. Prognostic Aspects*, Novosibirsk: Nauka, 1990, pp. 44–50.
54. Tenthorey, E., Cox, S.F., and Todd, H.F., Evolution of Strength Recovery and Permeability during Fluid-Rock Reaction in Experimental Fault Zones, *Earth Planet. Sci. Lett.*, 2003, vol. 206, pp. 161–172.
  55. Turcotte, D. and Schubert, J., *Geodynamics: Application of Continuum Physics to Geological Problems*, New York: John Wiley and Sons, 1982.
  56. Beeler, N. and Hickman, S., Stress-Induced, Time-Dependent Fracture Closure at Hydrothermal Conditions, *J. Geophys. Res.*, 2004, vol. 109. <https://doi.org/10.1029/2002JB001782>
  57. Niemeijer, A., Marone, C., and Elsworth, D., Healing of Simulated Fault Gouges Aided by Pressure Solution: Results from Rock Analogue Experiments, *J. Geophys. Res. B*, 2008, vol. 113, p. 04204. <https://doi.org/10.1029/2007JB005376>
  58. Tenthorey, E. and Cox, S.F., Cohesive Strengthening of Fault Zones during the Interseismic Period: An Experimental Study, *J. Geophys. Res. B*, 2006, vol. 111, p. 09202. <https://doi.org/10.1029/2005JB004122>
  59. Ikari, M.J., Carpenter, B.M., and Marone, C., A Microphysical Interpretation of Rate- and State Dependent Friction for Fault Gouge, *Geochem. Geophys. Geosyst.*, 2016, vol. 17, pp. 1660–1677. <https://doi.org/10.1002/2016GC006286>
  60. Chester, F.M. and Higgs, N.G., Multimechanism Friction Constitutive Model for Ultrafine Quartz Gouge at Hypocentral Locations, *J. Geophys. Res.*, 1992, vol. 97, pp. 1859–1870.
  61. Johnson, K.L., *Contact Mechanics*, Cambridge University Press, 1985.
  62. Popov, V.L., *Contact Mechanics and Friction. Physical Principles and Applications*, Berlin: Springer-Verlag, 2010.
  63. Batukhtin, I.V., Budkov, A.M., and Kocharyan, G.G., Features of Initiation and Rupture with Heterogeneous Fault Surfaces, in *Trigger Effects in Geosystem, Proc. of the V Int. Conf.*, 2019, pp. 137–149.
  64. Kocharyan, G.G. and Pavlov, D.V., Damage and Healing of Fault Zones in Rock, *Fiz. Mezomekh.*, 2007, vol. 10, no. 1, pp. 5–18.
  65. Uchida, N. and Burgmann, R., Repeating Earthquakes, *Annu. Rev. Earth Planet. Sci.*, 2019, vol. 47, pp. 305–332.
  66. Metois, M., Vigny, C., and Socquet, A., Interseismic Coupling, Megathrust Earthquakes and Seismic Swarms along the Chilean Subduction Zone (38°–18°S), *Pure Appl. Geophys.*, 2017, vol. 173, no. 5, pp. 1431–1449. <https://doi.org/10.1007/s00024-016-1280-5>
  67. Godano, M., Bernard, P., and Dublanchet, P., Bayesian Inversion of Seismic Spectral Ratio for Source Scaling: Application to a Persistent Multiplet in the Western Corinth Rift, *J. Geophys. Res. Solid Earth*, 2015, vol. 120, pp. 7683–7712. <https://doi.org/10.1002/2015JB012217>
  68. Matsuzawa, T., Igarashi, T., and Hasegawa, A. Characteristic Small-Earthquake Sequence off Sanriku, Northeastern Honshu, Japan, *Geophys. Res. Lett.*, 2002, vol. 29, no. 11, p. 1543. <https://doi.org/10.1029/2001GL014632>
  69. Okada, T., Matsuzawa, T., and Hasegawa, A., Comparison of Source Areas of  $M4.8 \pm 0.1$  Repeating Earthquakes off Kamaishi, NE Japan—Are Asperities Persistent Features?, *Earth Planet. Sci. Lett.*, 2003, vol. 213, pp. 361–374.
  70. Bie, L., Hicks, S., Garth, T., Gonzalez, P., and Rietbrock, A., ‘Two Go Together’: Near-Simultaneous Moment Release of Two Asperities during the 2016 Mw6.6 Muji, China Earthquake, *Earth Planet. Sci. Lett.*, 2018, vol. 491, pp. 34–42. <https://doi.org/10.1016/j.epsl.2018.03.033>
  71. Yamanaka, Y. and Kikuchi, M., Asperity Map along the Subduction Zone in Northeastern Japan Inferred from Regional Seismic Data, *J. Geophys. Res. B*, 2004, vol. 109, p. 07307. <https://doi.org/10.1029/2003JB002683>
  72. Freymueller, J.T., Cohen, S.C., and Fletcher, H.J., Spatial Variations in Present-Day Deformation, Kenai Peninsula, Alaska, and Their Implications, *J. Geophys. Res.*, 2000, vol. 105, pp. 8079–8101.
  73. Zhang, X.F., Wanpeng, H., Li, D., Wang, L., Shuai, Y., Wang, L., and Yongzhe, The 2018 Mw7.5 Papua New Guinea Earthquake: A Dissipative and Cascading Rupture Process, *Geophys. Res. Lett.*, 2020, vol. 47. <https://doi.org/10.1029/2020GL089271>